Effect of Short Chain Branching on the Blown Film Properties of Linear Low Density Polyethylene

YONG-MAN KIM and JUNG-KI PARK*

Department of Chemical Engineering, Korea Advanced Institute of Science and Technology, 373-1, Kusung-dong, Yusung-gu, Daejon 305-701, Korea

SYNOPSIS

Three linear low density polyethylene (LLDPE) resins of similar melt index and density were synthesized with different comonomers in the Unipol pilot-plant scale reactor. The molecular structure, blown film morphology, and film strength properties of the resins have been comprehensively characterized. The film dart drop impact strength of the LLDPEs increases in the order of ethylene/1-butene, ethylene/1-octene, and ethylene/1-hexene copolymers; whereas the Elmendorf tear strength of them increases in the order of ethylene/1-butene, ethylene/1-hexene, and ethylene/1-octene copolymers. The mechanical properties seem to be highly associated with the length and distribution of short chain branches and, consequently, the lamellar thickness distribution of the resins.

INTRODUCTION

Linear low density polyethylene (LLDPE) is a copolymer of ethylene and alpha olefin, such as 1-butene, 1-hexene, and 1-octene. The presence of small amounts of an alpha olefin introduces short chain branches on the polymer backbone. The major commercial use of LLDPEs is in blown film applications, and the mechanical properties of LLDPE films are generally known to be influenced by molecular structural parameters such as molecular weight, molecular weight distribution, and the type, amount, and distribution of short chain branches. In addition, the morphological features such as preferred orientation, stacked lamellar crystalline morphology, the degree of crystallinity, surface roughness, and intercrystalline connectivity, which are very sensitive to the processing conditions and molecular structure, are known to have a major effect on the mechanical properties of blown LLDPE films.[1-6]

The molecular weight and molecular weight distribution are usually fixed within a limited range for a specific application. Short chain branching is critical in affecting the morphology and, consequently, the solid-state properties of blown LLDPE films. Hence, a broad range of properties of blown LLDPE films can be obtained by simply varying branching characteristics. It is well known in the industry that the ethylene/1-octene LLDPEs have slightly better impact and tear strength compared to the ethylene/1-hexene LLDPEs, which in turn are more superior to the ethylene/1-butene LLDPEs of similar melt index and density. Nevertheless, relatively little has been reported on the details of the underlying mechanics for this phenomenon.

In this study, the three LLDPEs of similar melt index and density were synthesized with 1-butene, 1-hexene, and 1-octene as a comonomer in the Unipol pilot-plant scale reactor. The molecular structure, blown film morphology, and film dart drop impact and Elmendorf tear strengths of the resins have been comprehensively characterized. It is the purpose of this work to present some observations that may shed light on understanding of the origins of the differences in the mechanical properties of the three LLDPEs with different comonomer lengths.

* To whom correspondence should be addressed.

Journal of Applied Polymer Science, Vol. 61, 2315-2324 (1996)
 CCC 0021-8995/96/132315-10

EXPERIMENTAL

Materials

The three LLDPEs, labeled B, H, and O, used are listed in Table I. They were made by the copolymerization of the desired alpha olefin with ethylene in the Unipol pilot-plant scale reactor with the Ziegler–Natta catalyst. The melt indices and densities of all the samples are essentially comparable, ca. 0.95 g/10 min and 0.918 g/cm^3, respectively. The resins B, H, and O, contained 1-butene, 1-hexene, and 1-octene as a comonomer, respectively.

Characterization of Molecular Structure

High-temperature gel permeation chromatography (GPC) was carried out on a Waters 150CV instrument to determine the molecular weight distributions of the LLDPEs. 1,2,4 trichlorobenzene, containing 0.025% (*w/v*) Santanox R antioxidant, was used as the solvent. The operating temperature, flow rate, and injection volume were 145°C, 1 mL/min, and 250 μL, respectively. Characteristics of the columns were calibrated using National Bureau of Standards SRM 1476 polyethylene and narrow polystyrene standards.

The copolymer compositions of the LLDPEs were determined by ^{13}C NMR spectroscopy. The ^{13}C NMR spectra were recorded on a Bruker AMX 500 NMR spectrometer. The pulse angle, delay time, and scan number were 45°, 9.18 s, and 3000, respectively. Sample measurements were taken at 120°C. About 15% (*w/v*) of the sample solution in a mixed solvent of 80% (*v/v*) 1,2,4 trichlorobenzene and 20% (*v/v*) perdeuteriobenzene was measured. The observed chemical shifts were referenced to an internal hexamethylene disiloxane (HMDS) standard and corrected to tetramethylsilane (TMS) by adding 2.03 ppm.

Preparative temperature rising elution fractionation (preparative TREF) was performed to characterize the short chain branching distributions of the LLDPEs. Detailed information on preparative TREF technique was described elsewhere.[7] The LLDPE dissolved in BHT-antioxidant stabilized hot xylene at a concentration of 0.015 g LLDPE/cm^3 was crystallized from 132°C to room temperature at a rate of 1.2°C/h. The crystallized molecular species on glass beads were dissolved by heating at a rate of 10°C/h to the upper temperature of a desired range. After equilibrium at this temperature for 30 min, the solution was eluted with new solvent preheated to that temperature, and the eluted solution was collected as a fraction. The elution temperature ranges used in this study were as follows: below 55, 55–60, 60–65, 65–70, 70–75, 75–80, 80–85, 85–90, 90–95, 95–100, and 100–105°C. The yield of fractions eluted above 105°C was too poor to collect. The fractions were precipitated with acetone, filtered, washed with methanol, and then dried in vacuo at 50°C. The weights of the fractions were measured, and the molecular structures of them were characterized by the above procedures.

Blown Film Preparation

Films were prepared using a 40 mm Yoo Jin Engineering tubular blown LLDPE film equipment under

Table I Characteristics of the LLDPE Resins

Characteristics	Resin		
	B	H	O
Melt index[a] (g/10 min)	0.95	0.91	0.99
Density[b] (g/cm^3)	0.918	0.918	0.919
$\overline{M_n}$	35982	32986	31680
$\overline{M_w}$	214538	215265	199129
$\overline{M_w}/\overline{M_n}$	6.0	6.5	6.3
Comonomer	1-butene	1-hexene	1-octene
Mole fraction			
Ethylene	0.9566	0.9627	0.9719
Comonomer	0.0434	0.0373	0.0281
Branch frequency (CH_3/1000 C)	20.8	17.4	13.0
Monomer dispersity	86	92	95

[a] ASTM D 1238 (condition E).
[b] ASTM D 1505.

a commercially typical processing condition. It consists of a full flight screw with an L/D of 25 to 1, a 50 mm spiral die with a die gap of 2.3 mm, an air ring, nip rolls, and take-up device. The extrusion motor speed was fixed at 810 rpm; and the extrusion temperature was fixed at 160, 170, 180, 190, and 190°C for cylinder zones 1, 2, adapter, die 1, and die 2, respectively. The film thickness, blow-up ratio, and frost-line height were ca. 30 μm, 2.5 : 1, and 25 cm, respectively.

Characterization of the Morphology of Films

Pole figures of the crystallographic axes for the films were obtained using Rigaku D/MAX-IIIC(3 kW). Seventeen sheets of films were carefully stacked to give approximately 500 μm in total thickness. The specimens were cut from the stacks using a disk cutter with a diameter of 32 mm, and the edge of the disk specimens were glued with a water-based glue. All the X-ray measurements were performed using nickel filtered CuKα radiation produced at 40 kV and 45 mA. The Decker et al.[8] transmission and Schulz[9] reflection methods were used for low and high α angles, respectively. The connection angle was 30°. Measuring conditions were as follows: α angle variation, 0–90°; β angle variation, 0–360°; α and β angle step, 10°; β angle speed, 190°/min; and γ oscillation, 10 mm. The intensity data were corrected for background scattering and absorption.

The crystalline morphology of the films was observed by a scanning electron microscope, Phillips SEM 535M. The heptane-etched[10] specimens were sputter coated with approximately 100 Å of gold. Accelerating voltage, probe current, and tilt angle were 7 kV, 3×10^{-11} mA, and 30°, respectively.

The melting behaviors of the films were analyzed by differential scanning calorimetry (DSC) using the DuPont Thermal Analyst 2100 model at a heating rate of 10°C/min in nitrogen atmosphere. The melting endotherms were recorded by heating the samples from −10 to 160°C. The degree of crystallinity from the calorimetric data was calculated using 69 cal/g for the completely crystalline polyethylene.[11]

The lamellar thickness distribution was determined by analyzing the low-frequency Raman-active longitudinal acoustic vibrational modes of the films. The pole figure specimens were used again for the Raman spectroscopical experiment. Raman spectra were obtained using a Jovin-Yvon U1000 spectrometer fitted with 1800 grooves/mm double holographic gratings and PM tube (GaSe/Se doping) detector. The 514.5 nm Ar^+/Kr^+ mixed laser line was used for excitation. Scan time and laser power were 0.5 $cm^{-1}/2$ s and ca. 100 mW, respectively. Data were recorded at a spectral resolution of ca. 4 cm^{-1} using a slits 500-1000-1000-500 μm. The depolarizing scrambler was used to minimize the effects of the preferred chain orientation of the films.

The tie molecule densities of the films along the MD and TD were evaluated from brittle fracture stress measurements proposed by Brown and Ward.[12] The brittle fracture stresses of the films were measured using an Instron Testing Machine equipped with the modified grips. The ASTM D 1708 dogbone type tensile specimens were gripped firmly by the jaws, which were mounted inside the reservoir of liquid nitrogen. The specimens were conditioned for 10 min and deformed at a crosshead speed of 500 mm/min.

Mechanical Testing

Dart drop impact strength was measured according to ASTM D 1709 (method A). Elmendorf tear strength was determined by ASTM D 1922 (rectangular specimen).

RESULTS AND DISCUSSION

Molecular Characteristics

The molecular weight distributions of the three LLDPEs are shown in Figure 1, and the average

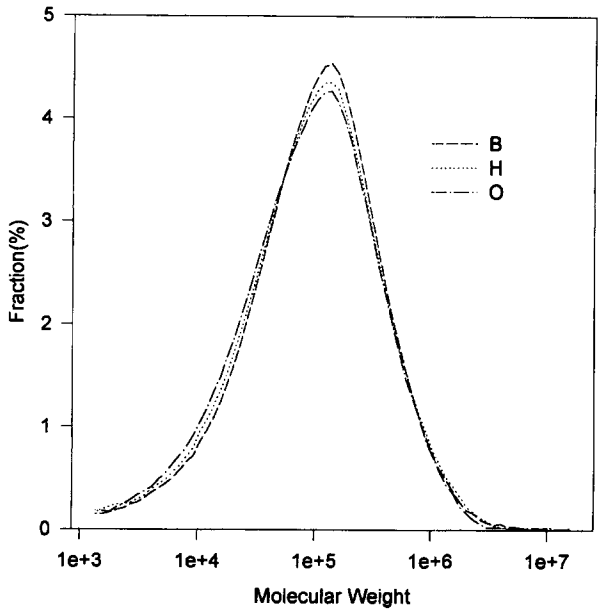

Figure 1 Gel permeation chromatograms of the LLDPE resins.

molecular weights and polydispersities of the resins are summarized in Table I. The average molecular weights and molecular weight distributions of all the resins are comparable, although the resin O has a slightly lower weight-average molecular weight than the others.

The branching characteristics of the LLDPEs were determined by ^{13}C NMR spectroscopy in the conventional manner.[13] The quantitative ^{13}C NMR analysis of branching in polyethylene has been a subject of much investigation due to the commercial importance of this material.[13-16] The assignments are well-established at present for the products containing less than 10 mol % of the comonomer. The ^{13}C NMR results such as comonomer type, composition, branch frequency, and monomer dispersity of the resins are also listed in Table I. The monomer dispersity is the ratio of the sequence number to the total comonomer content and represents the tendency of the comonomer units to form contiguous series.[13,14] The LLDPEs B, H, and O contained 4.3 mol % 1-butene, 3.7 mol % 1-hexene, and 2.8 mol % 1-octene, respectively. The branch frequency per 1000 carbon atoms and monomer dispersity are 20.8 and 86, respectively, for the resin B, 17.4 and 92 for the resin H, and 13.0 and 95 for the resin O. The monomer dispersities of all the resins are less than those predicted for a Bernoullian distribution of the same composition. This indicates that the LLDPEs are intraheterogeneous. It is clear from the ^{13}C NMR results that the longer branched LLDPE shows lower average short chain branching content and comonomer blockiness, although the densities of the resins are very similar.

The separation of a polymer material into its component molecular species constitutes the most important step in any detailed polymer structure study. Through subsequent analysis of the resultant fractions one develops a knowledge of the nature of the complex parent material. The LLDPE resins were fractionated into eleven fractions via preparative TREF technique, and the detailed molecular structures of the fractions have been characterized using GPC and ^{13}C NMR spectroscopy.

The TREF distributions of the LLDPEs which represent the relation between average elution temperature, defined as the midpoint of the elution temperature interval, and the weight percentage of the fractions are shown in Figure 2. These materials would be characterized by an extremely broad and multimodal short chain branching distribution. This was the characteristic of the conventional LLDPEs presented previously.[5,17-21] The distribution of molecular species present in the LLDPEs could be subdivided into three components in the conventional manner: (1) polyethylene with lower short chain branching content, which corresponds to the fractions eluted above 90°C, i.e., high density polyethylene (HDPE)-like component; (2) polyethylene having branch frequency similar to that of the whole polymer; and (3) polyethylene with much higher short chain branching content eluted below 60°C. For the resins B, H, and O, the amounts of the HDPE-like component were 17.0, 28.1, and 31.3 wt %; and those of the component with much higher branching were 28.6, 28.9, and 30.2 wt %, respectively. Several workers[5,18,20,22,23] have introduced that a homogeneity of the short chain branching distribution can be quantified by the relative amount of HDPE-like component or the sum of HDPE-like and much higher branching components. According to this idea, the interheterogeneity of short chain branching of the LLDPEs in descending order is O > H > B.

From the results of mass percentage, average short chain branching content, and molecular weight distribution of the fractions, the dependence of short chain branching content on molecular weight for the LLDPEs was calculated and is given in Figure 3. The short chain branching distribution of all the resins with molecular weight does not seem to be much different from each other.

Morphological Features

The molecular orientation imparted during blown film preparation is known to have a profound effect on the mechanical properties of LLDPEs. The development of molecular orientation in the crystalline phase of blown LLDPE film can be conveniently determined by investigating the alignment of its unit cell. Figures 4 and 5 show the normalized intensity profiles of (200) and (020) poles, i.e., a- and b-axis distributions, as a function of α and β angles. The sample reference directions, machine direction (MD), transverse direction (TD), and normal direction (ND), are noted in the figure captions. In these figures, the major tick mark of the abscissa indicates α angle variations from 0 to 90°, and the minor tick mark indicates β angle variations from 0 to 350° at a given α angle. There is no significant differences in the intensity profiles of (200) and (020) poles between the three films. The a-axes are somewhat preferentially oriented to the MD than to the TD and ND. This indicates that the orientation occurred under the low-stress crystallization proposed by Maddams and Preedy.[24] The b-axes of the films are

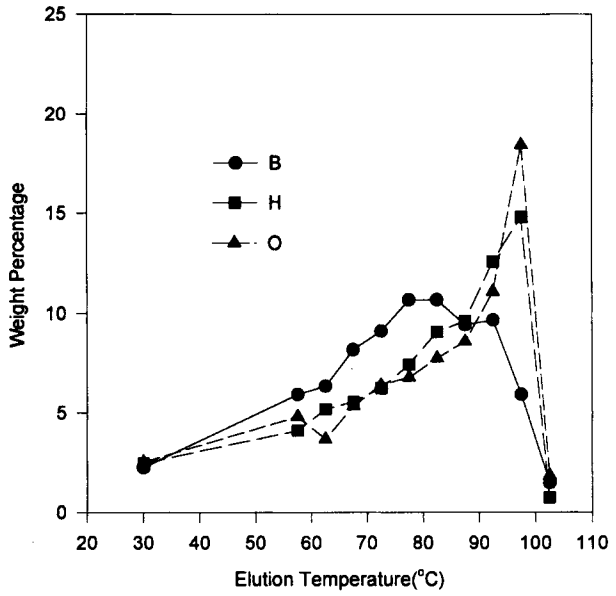

Figure 2 Short chain branching distributions of the resins.

mostly perpendicular to the MD and have a preferential orientation to the ND in the TD-ND plane.

The mean-square cosines of the angle, $\langle \cos^2\psi_{i,j} \rangle$, between a crystallographic axis (i = a- and b-axis) of orthorhombic crystallite of polyethylene and the sample reference directions (j = ND, MD, TD) were calculated by the well-known method[25,26]; and the mean-square cosines of the angle between c-axis and the sample reference directions, $\langle \cos^2\psi_{c,j} \rangle$, were calculated from $\langle \cos^2\psi_{a,j} \rangle + \langle \cos^2\psi_{b,j} \rangle + \langle \cos^2\psi_{c,j} \rangle = 1$. The dichroic ratios defined as $\langle \cos^2\psi_{i,j=\mathrm{MD}} \rangle / \langle \cos^2\psi_{i,j=\mathrm{TD}} \rangle$ were calculated from the mean-square cosines. There is no significant differences in the dichroic ratios of all the films, as shown in Table II.

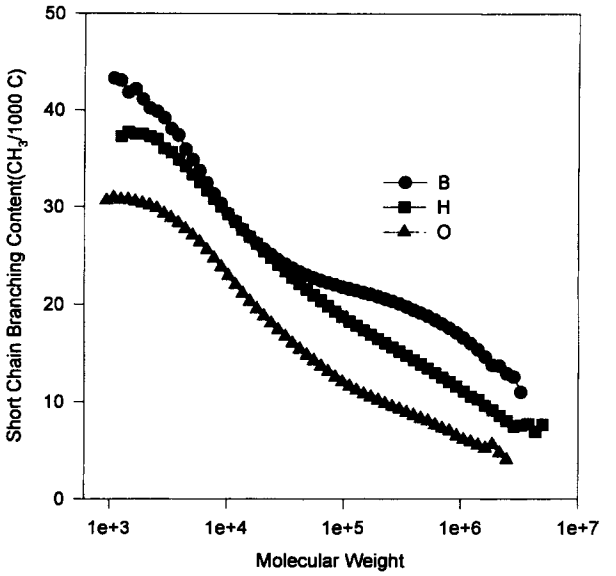

Figure 3 Dependence of short chain branching content on the molecular weight for the LLDPE resins.

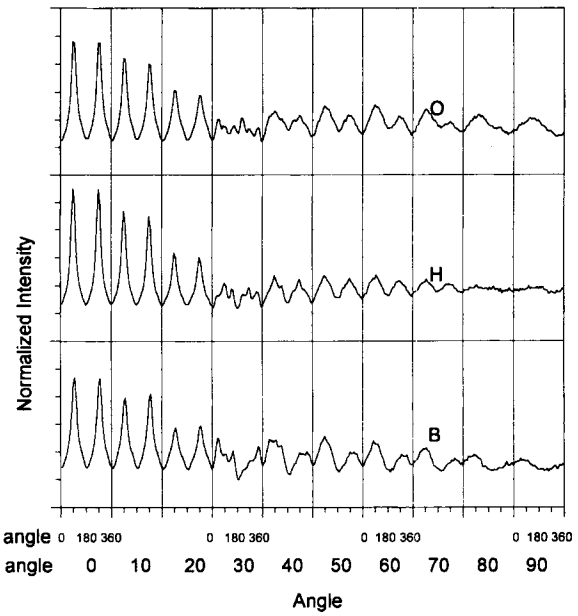

Figure 4 Intensity of (200) pole against α and β angles. (MD: α = 0; β = 90 or 270°. TD: α = 0; β = 0 or 180°. ND: α = 90°.)

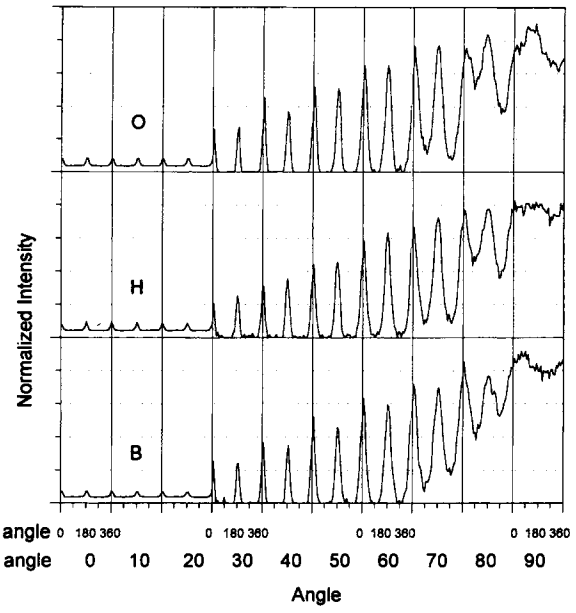

Figure 5 Intensity of (020) pole against α and β angles. (MD: α = 0, β = 90 or 270°. TD: α = 0, β = 0 or 180°. ND: α = 90°.)

Table II Dichroic Ratios (MD/TD) of Crystallographic Axes

	Dichroic Ratio ($\langle\cos^2\psi_{i,MD}\rangle/\langle\cos^2\psi_{i,TD}\rangle$)		
Film	a-axis	b-axis	c-axis
B	1.49	0.31	1.07
H	1.52	0.34	1.06
O	1.49	0.29	1.09

The typical scanning electron micrographs of the normal planes for the films are presented in Figure 6. The MD and TD are vertical and horizontal directions of micrographs, respectively. Crystals appeared as bright areas. The low magnification (×2000) micrographs clearly reveal the surface morphology, and the lamellar structures of the films are well shown in the higher magnification (×20,000) micrographs taken by zooming up around an area in the micrographs of ×2000 magnification. Firdaus and Tong[4] have demonstrated that the melt fracture has a strong influence on the blown film properties of LLDPE resin, and the poor mechanical properties were obtained for rougher films produced at the same extrusion. The difference in surface roughness of the three LLDPE films is small, as revealed in Figure 6(a), (c), and (e). It is also found from these micrographs that there is no evidence of the presence of a dispersed second soft phase, which was extractable with a weak solvent, in a hard semicrystalline matrix. Mirabella et al.[10] have suggested that this very low crystalline second soft phase arises from the extreme compositional heterogeneity of LLDPE resins, performs a function similar to that of the rubberlike second phase in other high impact resins, and thus leads to the observed extraordinary fracture toughness of LLDPE resins. The reason for the absence of the second phase of the blown films used in this study can be primarily attributed to the faster crystallization rate compared to that of the compression-molded plaques which Mirabella et al.[10] have investigated. Figures 6(b), (d), and (f) show the lamellar structures of the B, H, and O films, respectively. All the films reveal similar lateral extent (length) and orientation distribution of the lamellae. The lateral extent of lamellae, the contrast between amorphous and crystalline regions, and the extents of the crystallites of the films are more significantly reduced than those of the blown HDPE films presented in the previous study.[27] This would be attributed mainly to higher short chain branching content of the LLDPEs compared to the HDPEs, since branches disrupt chain regularity and thus interrupt the crystallization process. This feature is consistent with the previously cited observations in the compression-molded plaques[28] and the oriented thin films.[29] The normals of the lamellae are randomly oriented in the plane of the LLDPE films. Contrary to the blown HDPE films, it is very difficult to evaluate the organization of lamellar stacks from the images of the normal plane of the LLDPE films since the boundary between lamellar stacks are not well defined. Thus, we observed the detailed morphology of the dart drop impact failure regions using scanning electron microscopy (SEM) to investigate the superstructure. Figure 7 shows the images of the dart drop impact failure regions of the films. The morphologies of the underformed regions of the B and H films are shown at the right sides of the micrographs presented in Figure 7(a) and (b), respectively. The left side of the micrograph given in Figure 7(c) reveals the morphology of the undeformed region of the O film. These micrographs clearly show the organization of the lamellar stacks of the LLDPE films. The normals of the lamellar stacks of all the films have a higher preferential orientation to the MD. These micrographs also reveal the deformation behavior of the films resulting from impact of a free-falling dart. The lamellar stacks are separated and then rotated perpendicular to the failure boundary line, as shown at the left sides of the Figure 7(a) and (b) and at the right side of the Figure 7(c). The fragmentation of lamellar stacks and the axial deformation of the reoriented lamellar stacks were also found in these micrographs.

The melting behavior of the films was studied with a differential scanning calorimeter. The melting endotherms of the films are given in Figure 8. There is no significant difference in the degree of crystallinity (38–39%). However, the melting behaviors are very different among the films, suggesting differences in crystal size distributions. The peak melting temperature of the films increases when the comonomer length increases in the order of the 1-butene, 1-hexene, and 1-octene; while the distribution of endotherms for them becomes more heterogeneous, as can be shown by the idea on the homogeneity of short chain branching distribution proposed by several workers.[5,18,20,22,23] This would be associated primarily with the short chain branching distributions of the LLDPEs, as shown in Figure 2. In order to compare more directly the lamellar thickness distributions, we have investigated the low-frequency Raman-active longitudinal acoustic vibrational modes of the films. The ob-

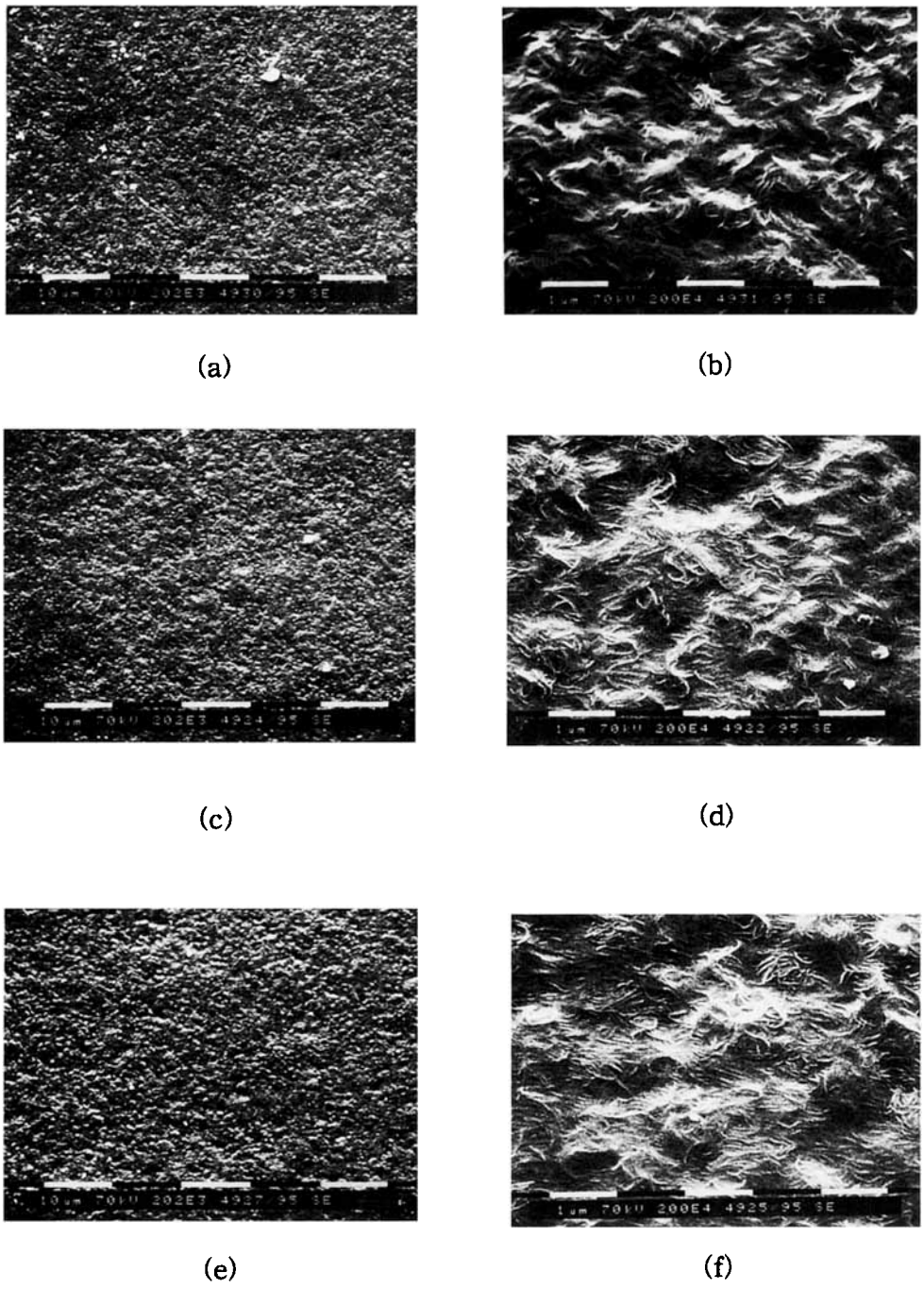

Figure 6 Scanning electron micrographs of the normal plane of the films (MD ↑, TD →): (a) B, ×2000; (b) B, ×20,000; (c) H, ×2000; (d) H, ×20,000; (e) O, ×2000; and (f) O, ×20,000.

served Raman spectra, not corrected for the frequency and temperature due to the lower intensity, are shown in Figure 9. The apparent peak frequencies are indicated by arrows. The observed intensities of the films are spread out over a larger frequency range, and some merging of them with background is also found. This represents the broad complex lamellar thickness distribution, as was already indicated by Voight-Martin and Mandelkern.[30] Although this complex distribution makes the quantitative resolution difficult, the difference in the lamellar thickness distribution of the films postulated from the DSC melting endotherms is partially supported.

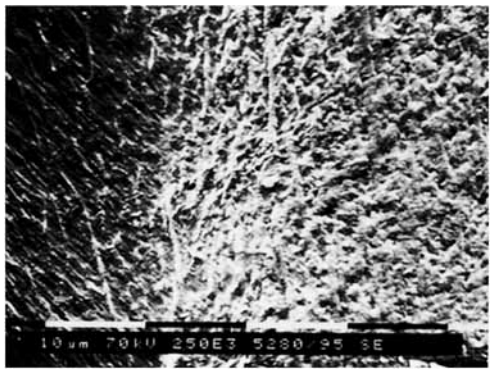

(a)

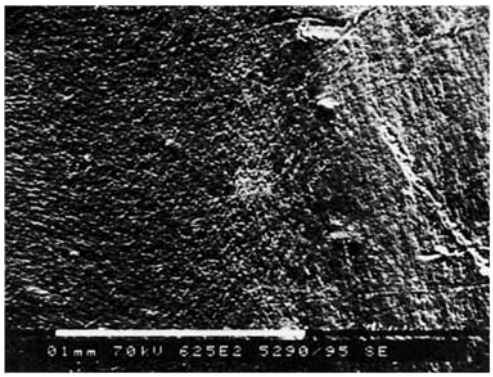

(b)

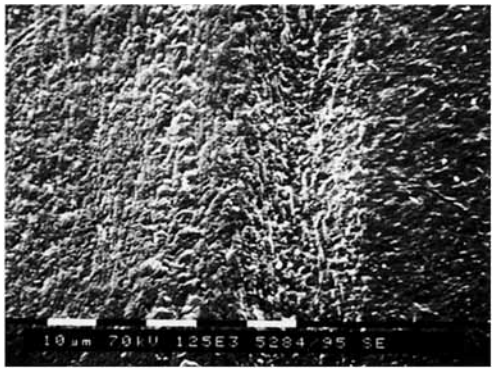

(c)

Figure 7 Scanning electron micrographs of the dart drop impact failure region of the films (MD ↑, TD →): (a) B, ×2500; (b) H, ×625; and (c) O, ×1250.

The brittle fracture tensile stress of the films was measured to evaluate the relative tie molecule density of the films.[12] The brittle fracture stress and calculated tie molecule density of the films are listed in Table III. Their differences among the films are imperceptible. For all the films, the intercrystalline connectivity along the MD is higher than that along the TD due to the higher preferential orientation of the lamellar stacks to the MD.

Mechanical Properties

The dart drop impact strength data on all the films are given in Table IV. The dart drop impact strength of the LLDPE films decreases in the order of H, O, and B. This trend is different from the well-known fact in the industry that for the commercial LLDPEs, the impact strength decreases in the order of ethylene/1-octene, ethylene/1-hexene, and ethylene/1-butene LLDPEs. The most common explanation of the superior properties of a longer branched LLDPE is that a longer short chain branch is more excluded from the crystal lamellae, and the chains then reside in the amorphous and interfacial regions, thus favoring the formation of tie molecules.[20,21,31,32] However, considering the results of this study, this premise is not sound in interpreting the differences in dart drop impact strengths of the B, H, and O films. The differences in dart drop impact strengths of the three films also cannot be explained in terms of the second soft phase. Furthermore, they cannot be explained by the differences in the surface roughness and the preferred orientations of the

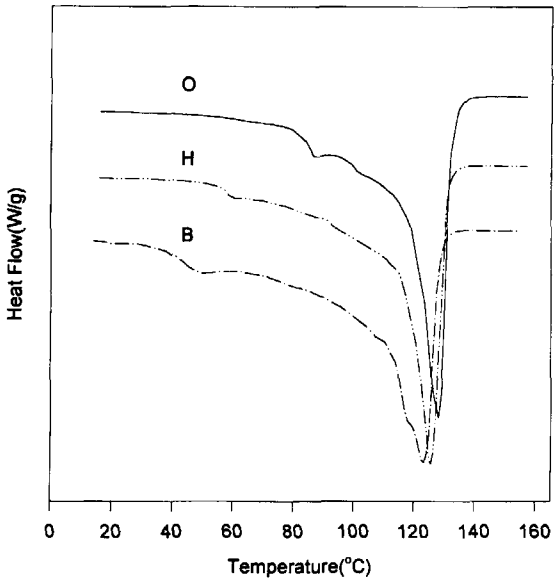

Figure 8 DSC melting endotherms of the films.

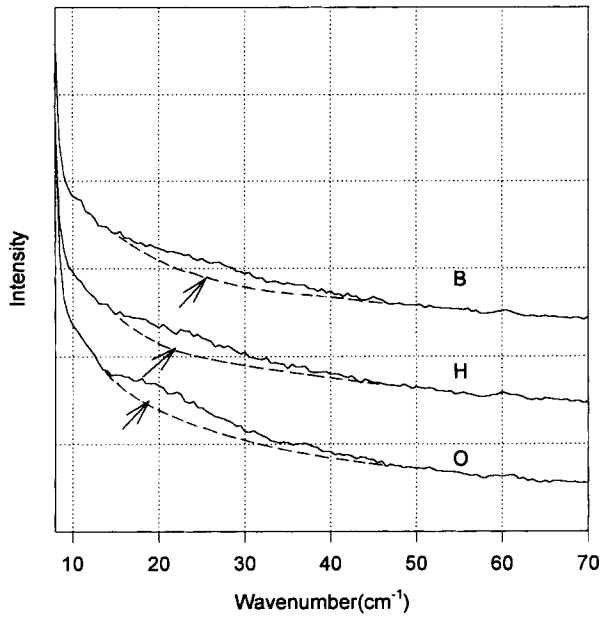

Figure 9 Low-frequency Raman spectra of the films.

crystallographic axes, lamellae, and lamellar stacks, which are generally known to have a major effect on the mechanical properties of blown LLDPE films. As demonstrated in the previous section, these parameters are very similar among the B, H, and O films. The dart drop impact failure of the films was proceeded by initial separations and subsequent reorientations of lamellar stacks resulting in the many microfibrils between intra- and interstacks and the fragmentation of the lamellar stacks, as was referred previously. This failure behavior is very similar to the tensile deformation behavior of lamellar stacks observed by Sherman.[33] The impact failure behavior suggests that the dart drop impact strength of the films would be correlated highly with the stability

Table IV Mechanical Properties of the Films

Film	B	H	O
Dart drop impact strength (g)	72	193	129
Elmendorf tear strength (g)			
MD	77	237	246
TD	557	922	1251
TD/MD	7.2	4.2	5.1

of the lamellar stacks and, thus, probably related to the degree of internal crystallographic imperfection and lamellar thickness distribution. Short chain branches are known to be incorporated into a crystal lattice for melt quenched polyethylene. The extent of incorporation increases with increasing the degree of branching and with decreasing the bulkiness of branch.[20,21,34] Therefore, the resin B is expected to have more internal crystallographic imperfection than the others and, thus, to produce the film with lower impact strength. The lamellar thickness distribution was found to be the only morphological parameter that is significantly different among the B, H, and O films, which would be primarily associated with the short chain branching distribution of the LLDPEs. Lee et al.[3] have reported that the development of a smaller and finer crystalline domain morphology appears to give a better impact strength and more balanced tear strength properties due to better distribution of stress. The smaller lamellae and more homogeneous lamellar thickness distribution resulting from the narrower short chain branching distribution would be responsible for the higher impact strength of the H film compared to the O film. Crotty and Firdaus[5] have also reported

Table III Brittle Fracture Stress and Calculated Tie Molecule Density of the Films

Film		Brittle Fracture Stress (GPa)	Tie Molecule Density (Fraction)[a] β = 0.1, c = 20	β = 0.1, c = 50	β = 0.2, c = 20	β = 0.2, c = 50
B	MD	0.1359	0.0657	0.2053	0.0191	0.0890
	TD	0.1142	0.0508	0.1682	0.0117	0.0704
H	MD	0.1368	0.0663	0.2068	0.0195	0.0897
	TD	0.1219	0.0561	0.1813	0.0143	0.0770
O	MD	0.1309	0.0623	0.1967	0.0174	0.0847
	TD	0.1160	0.0521	0.1723	0.0123	0.0719

[a] Tie molecule density,[12] $f_T = (C\sigma_F - \beta E_{iso})/\beta\ (E_T - E_{iso})$, where C is the stress concentration, σ_F is brittle fracture stress, β is the constant of proportionality, and E_{iso} and E_T are the Young's modulus for van der Waals' bonds (8GPa) and tie molecule (300GPa), respectively.

that the super strength ethylene/1-hexene LLDPEs which are characterized by the narrower short chain branching distribution produced films with impact and tear strengths significantly higher than the conventional ethylene/1-hexene LLDPEs and even higher than the ethylene/1-octene LLDPEs. Thus, the apparent discrepancy in the film dart drop impact strength of ethylene/1-hexene and ethylene/1-octene LLDPEs between the conventional LLDPEs and the LLDPEs used in this study can be primarily attributed to the differences in short chain branching distributions. On the other hand, the lamellae are suspected to be too small to enhance the dart drop impact resistance of the B film.

From the above morphological and microstructural considerations we have so far, it may be suggested that the film dart drop impact strength of the LLDPEs of similar melt index and density is significantly dominated by the length and distribution of short chain branches.

The Elmendorf tear strength values in the MD and TD of the films are listed in Table IV. For all the films, the TD Elmendorf tear strength exceeds the MD Elmendorf tear strength due to the higher preferential orientation of lamellar stacks to the MD. A tear in the MD experiences less resistance compared to the TD due to crystal cleavage and lower concentration of tie molecules. The Elmendorf tear strength increases in the order of B, H, and O. The differences in the Elmendorf tear strengths among the films appear to be associated with the degree of internal crystallographic imperfection and lamellar thickness of the films.

Support of this work by Hanwha Chemical Corporation is gratefully acknowledged.

REFERENCES

1. A. Haber and M. R. Kamal, *Proc. ANTEC '87,* 446 (1987).
2. C. Lee, I. Peat, L. Wild, and A. Fernando, *Proc. ANTEC '88,* 183 (1988).
3. C. Lee, I. Peat, L. Wild, and A. Fernando, *Proc. ANTEC '88,* 591 (1988).
4. V. Firdaus and P. P. Tong, *J. Plast. Film & Sheeting,* **8,** 333 (1992).
5. V. J. Crotty and V. Firdaus, *Proc. ANTEC '93,* 1210 (1993).
6. R. M. Patel, T. I. Butler, K. L. Walton, and G. W. Knight, *Polym. Eng. Sci.,* **34,** 1506 (1994).
7. Y. M. Kim, C. H. Kim, J. K. Park, J. W. Kim, and T. I. Min, *J. Appl. Polym. Sci.,* to appear.
8. B. F. Decker, E. T. Asp, and D. Harker, *J. Appl. Phys.,* **19,** 388 (1948).
9. L. G. Schulz, *J. Appl. Phys.,* **20,** 1033 (1949).
10. F. M. Mirabella, Jr., S. P. Westphal, P. L. Fernando, E. A. Ford, and J. G. Williams, *J. Polym. Sci. Polym. Phys. Ed.,* **26,** 1995 (1988).
11. P. J. Flory and A. Vrij, *J. Am. Chem. Soc.,* **85,** 3548 (1963).
12. N. Brown and I. M. Ward, *J. Mater. Sci.,* **18,** 1405 (1983).
13. J. C. Randall, *J. Macromol. Sci. Rev. Macromol. Chem. Phys.,* **C29,** 201 (1989).
14. E. T. Hsieh and J. C. Randall, *Macromolecules,* **15,** 1402 (1982).
15. T. Usami and S. Takayama, *Macromolecules,* **17,** 1756 (1984).
16. M. De Pooter, P. B. Smith, K. K. Dohrer, K. F. Bennett, M. D. Meadows, C. G. Smith, H. P. Schouwenaars, and R. A. Geerards, *J. Appl. Polym. Sci.,* **42,** 399 (1991).
17. L. Wild, T. R. Ryle, D. C. Knobeloch, and I. R. Peat, *J. Polym. Sci. Polym. Phys. Ed.,* **20,** 441 (1982).
18. E. Karbashewski, L. Kale, A. Rudin, W. J. Tchir, D. G. Cook, and J. O. Pronovost, *J. Appl. Polym. Sci.,* **44,** 425 (1992).
19. F. M. Mirabella Jr. and E. A. Ford, *J. Polym. Sci. Polym. Phys. Ed.,* **25,** 777 (1987).
20. S. Hosoda, *Polym. J.,* **20,** 383 (1988).
21. Xiao-Qi Zhou and J. N. Hay, *Eur. Polym. J.,* **29,** 291 (1993).
22. R. Benavente, J. M. Perena, A. Bello, E. Perez, C. Aguilar, and M. C. Martinez, *J. Mater. Sci.,* **25,** 4162 (1990).
23. E. Perez, R. Benavente, A. Bello, J. M. Perena, C. Aguilar, and M. C. Martinez, *Polym. Eng. Sci.,* **31,** 1189 (1991).
24. W. F. Maddams and J. E. Preedy, *J. Appl. Polym. Sci.,* **22,** 2751 (1978).
25. Z. W. Wilchinsky, *J. Appl. Phys.,* **31,** 1969 (1960).
26. L. E. Alexander, *X-ray Diffraction Methods in Polymer Science,* Wiley, New York, 1969.
27. Y. M. Kim, C. H. Kim, J. K. Park, J. W. Kim, and T. I. Min, *J. Appl. Polym. Sci.,* to appear.
28. I. G. Voight-Martin, R. Alamo, and L. Mandelkern, *J. Polym. Sci. Polym. Phys. Ed.,* **24,** 1283 (1986).
29. J. M. Brady and E. L. Thomas, *J. Polym. Sci., Polym. Phys. Ed.,* **26,** 2385 (1988).
30. I. G. Voight-Martin and L. Mandelkern, *J. Polym. Sci. Polym. Phys. Ed.,* **27,** 967 (1989).
31. S. W. Tsui, R. A. Duckett, and I. M. Ward, *J. Mater. Sci.,* **27,** 2799 (1992).
32. T. M. Liu and W. E. Baker, *Polym. Eng. Sci.,* **32,** 944 (1992).
33. E. S. Sherman, *Polym. Eng. Sci.,* **24,** 895 (1984).
34. P. Smith and R. St. J. Manley, *Macromolecules,* **12,** 483 (1979).

Received January 26, 1996
Accepted April 7, 1996